J|A|C|S
ARTICLES
Published on Web 11/23/2004

Crystalline, Mixed-Valence Manganese Analogue of Prussian Blue: Magnetic, Spectroscopic, X-ray and Neutron Diffraction Studies

Patrick Franz,[†] Christina Ambrus,[†] Andreas Hauser,[‡] Dmitry Chernyshov,[†,§] Marc Hostettler,[†] Jürg Hauser,[†] Lukas Keller,[∥] Karl Krämer,[†] Helen Stoeckli-Evans,[#] Philip Pattison,[⊥] Hans-Beat Bürgi,[†] and Silvio Decurtins[†,*]

Contribution from the Departement für Chemie und Biochemie und Laboratorium für Kristallographie, Universität Bern, Freiestrasse 3, CH-3012 Bern, Switzerland

Received June 11, 2004; E-mail: decurtins@iac.unibe.ch

Abstract: The compound of stoichiometry $Mn(II)_3[Mn(III)(CN)_6]_2 \cdot zH_2O$ ($z = 12-16$) (**1**) forms air-stable, transparent red crystals. Low-temperature single crystal optical spectroscopy and single crystal X-ray diffraction provide compelling evidence for N-bonded high-spin manganese(II), and C-bonded low-spin manganese(III) ions arranged in a disordered, face-centered cubic lattice analogous to that of Prussian Blue. X-ray and neutron diffraction show structured diffuse scattering indicative of partially correlated (rather than random) substitutions of $[Mn(III)(CN)_6]$ ions by $(H_2O)_6$ clusters. Magnetic susceptibility measurements and elastic neutron scattering experiments indicate a ferrimagnetic structure below the critical temperature $T_c = 35.5$ K.

Introduction

The mixed-valence iron(III)hexacyanoferrate(II) compound of composition $Fe_4[Fe(CN)_6]_3 \cdot zH_2O$ ($z = 14-16$), called Prussian Blue (PB), is considered to be one of the first synthetic coordination compounds.[1] Its metal-substituted analogues attract renewed and growing interest by chemists as well as physicists due to unique combinations of magnetic and optical properties.[2,3] These properties arise from a crystal structure that tolerates magnetic ions of different sizes and electronic spins, limits superexchange interactions to those across CN-bridges,[4] and thus allows tuning of magnetism and color. Current research efforts focus on PB analogues exhibiting spontaneous magnetization at comparatively high temperatures, as for instance $V(II)_{0.42}V(III)_{0.58}[Cr(III)(CN)_6]_{0.86} \cdot 2.8H_2O$,[5a,b] or on those combining magnetic with magnetooptical and electrochemical properties, as for instance $[Cr(II,III)_{2.12}(CN)_6]_n \cdot zH_2O$ which shows electrochemically tunable magnetic phase transitions.[6] Furthermore, photoinduced magnetization is found in $K_{0.2}Co_{1.4}[Fe(CN)_6] \cdot 6.9H_2O$[7a,b] and related systems.[8a,b] A further point is that all compounds mentioned here are structurally disordered resulting in some cases in ill-defined stoichiometries and poor crystallinity.[9-11] Elaborate theoretical analyses suggest an important role for local disorder in determining photomagnetic properties.[12,13] Experimental studies as function of chemical composition have shown that structural defects, namely $M(CN)_6$ vacancies filled by $(H_2O)_6$ clusters, are a prerequisite for photomagnetism.[14,15] The influence of the defects on the statistical distribution of the MN_nO_{6-n} configurations were deduced from Mössbauer experiments.[16] However, there is no information about spatial distribution of structural defects. This information can be obtained from combined measurement of accurate Bragg intensities and modulated diffuse scattering.[17]

[†] Departement für Chemie und Biochemie und Laboratorium für Kristallographie, Universität Bern, Freiestrasse 3, CH- 3012 Bern, Switzerland FAX: +41 31 631 39 95.
[‡] Département de Chimie Physique, Université de Genève, Quai Ernest-Ansermet 30, CH-1211 Genève 4, Switzerland.
[§] Petersburg Nuclear Physics Institute, St. Petersburg, Gatchina, 188350, Russia.
[∥] Labor für Neutronenstreuung, ETHZ & PSI, CH-5232 Villigen PSI, Switzerland.
[#] Institut de Chimie, Université de Neuchâtel, Av. de Bellevaux 51, CH-2000 Neuchâtel, Switzerland.
[⊥] Swiss Norwegian Beam Line at European Synchrotron Research Facility, BP 220, F-38043 Grenoble, CEDEX, France.

(1) Anonymous, *Miscellanea Berolinensia ad Incrementum Scientarium (Berlin)* **1710**, *1*, 377.
(2) Verdaguer, M.; Galvez, N.; Garde, R.; Desplanches, C. *Electrochem. Soc. Interface* **2002**, *11(3)*, 28.
(3) Ohkoshi, S.; Hashimoto, K. *Electrochem. Soc. Interface* **2002**, *11(3)*, 34.
(4) Verdaguer, M.; Bleuzen, A.; Marvaud, V.; Vaissermann, J.; Seuleiman, M.; Desplanches, C.; Scuiller, A.; Train, C.; Garde, R.; Gelly, G.; Lomenech, C.; Roseman, I.; Veillet, P.; Cartier, C.; Villain, F. *Coord. Chem. Rev.* **1999**, *192*, 1023.
(5) (a) Ferlay, S.; Mallah, T.; Ouahès, R.; Veillet, P.; Verdaguer, M. *Nature* **1995**, *378*, 701. (b) Kahn, O. *Nature* **1995**, *378*, 667.
(6) Sato, O.; Iyoda, T.; Fujishima, A.; Hashimoto, K. *Science* **1996**, *271*, 49.
(7) (a) Sato, O.; Iyoda, T.; Fujishima, A.; Hashimoto, K. *Science* **1996**, *272*, 704. (b) Verdaguer, M. *Science* **1996**, *272*, 698.
(8) (a) Champion, G.; Escax, V.; Cartier dit Moulin, C.; Bleuzen, A.; Villain, F.; Baudelet, F.; Dartyge, E.; Verdaguer, M. *J. Am. Chem. Soc.* **2001**, *123*, 12544; (b) Shimamoto, N.; Ohkoshi, S.; Sato, O.; Hashimoto, K. *Inorg. Chem.* **2001**, *41*, 678.
(9) Entley, W. R.; Girolami, G. S. *Inorg. Chem.* **1994**, *33*, 5165.
(10) Entley, W. R.; Girolami, G. S. *Science* **1995**, *268*, 397.
(11) Holmes, S. M.; Girolami, G. S. *J. Am. Chem. Soc.* **1999**, *121*, 5593.
(12) Kawamoto, T.; Asai, Y.; Abe, S. *Phys. Rev. B* **1999**, *60*, 12990.
(13) Kawamoto, T.; Asai, Y.; Abe, S. *Phys. Rev.* Lett. **2001**, *86*, 348.
(14) Bleuzen, A.; Lomenech, C.; Escax, V.; Villain, F.; Varret, F.; Cartier dit Moulin, C.; Verdaguer, M. *J. Am. Chem. Soc.* **2000**, *122*, 6648.
(15) Goujon, A.; Varret, F.; Escax, V.; Bleuzen, A.; Verdaguer, M. *Polyhedron* **2001**, *20*, 1339.
(16) Ksenofontov, V.; Levchenko, G.; Reiman, S.; Gütlich, P.; Bleuzen, A.; Escax, V.; Verdaguer, M. *Phys. Rev. B* **2003**, *68*, 024415.

10.1021/ja0465451 CCC: $27.50

Experimental studies of the dynamic susceptibility of the photoinduced magnetism in $K_{1-2x}Co_{1+x}[Fe(CN)_6]\cdot yH_2O$ revealed that compositional disorder leads to spin frustration and clustering of defects resulting in a magnetic cluster glass state.[18]

According to previous diffraction studies,[19,20] the structure of a generic PB-like compound $A\{[B(CN)_6]_x\cdot(6H_2O)_{1-x}\}\cdot yH_2O$ consists of two interpenetrating F-centered sub-lattices. All nodes of one of the sub-lattices are occupied by A cations, while those of the other sub-lattice are occupied by either $[B(CN)_6]$ anions or by $(H_2O)_6$ clusters. The details depend on the oxidations states of the A and B cations: for A(II) and B(III), $x = 2/3$, while for A(III) and B(II), $x = 3/4$. Every B cation is linked via C−N groups to six A cations and every A cation is surrounded (on average) by $6x$ $[B(CN)_6]$ complexes and by $6(1 - x)$ H_2O molecules. Additional water molecules (zeolitic water) may sit in structural cavities. The magnetic superexchange interactions between metal ions A and B are mediated by the cyano-bridges. If the spin-containing orbitals of magnetic ions are of the same symmetry, the spins couple antiferromagnetically, if the orbitals are orthogonal then ferromagnetic coupling occurs.[4] Variation of the A and B cations and concomitant introduction of $(H_2O)_6$ clusters thus change the type, strength and 3D topology of the magnetic coupling.

It is important to bear in mind that all structural characteristics derived from a Bragg diffraction experiment on a disordered crystal are average values and do not necessarily reflect local structure, such as actual bond lengths and angles. It is only the average structure of most PB analogues that has been well established by X-ray single crystal and powder diffraction studies.[19,20] Considering that magnetic interactions are defined by the spatial arrangement of magnetic centers, i.e., by the *local* crystal structure, disorder is a serious problem in the structural and magnetic characterization of PB-analogues. To our knowledge, disorder has not been studied experimentally so far, nor have microscopic magnetic structures, usually suggested on the basis of macroscopic magnetization measurements, been probed directly by an appropriate diffraction method.

In the present study we report magnetic, spectroscopic and structural properties of $Mn_3[Mn(CN)_6]_2\cdot zH_2O$ (**1**), a PB analogue with good crystallinity. We combine different probes such as single-crystal optical spectroscopy, single-crystal X-ray diffraction, multi-temperature neutron powder diffraction and SQUID measurements of bulk magnetization as a function of temperature and magnetic field. With this combination of techniques we identify the oxidation states of the Mn ions and the stoichiometry of **1**, characterize its average crystal and magnetic structures, and observe effects related to structural disorder. Finally, we list some open problems concerning the properties of PB analogues and suggest ways to investigate them.

Results and Discussion

Stoichiometry and Oxidation States. For PB analogues with A═B═Mn, three oxidation schemes have been reported: $Mn(II)[Mn(III)(CN)_6]_{2/3}$,[19] $Mn(II)[Mn(IV)(CN)_6]$,[21] and $Mn(III)[Mn(III)(CN)_6]$[22] with different amounts of structural and zeolitic water. In this study, the stoichiometry of **1** and the oxidation states of the Mn ions have been characterized by spectroscopy and diffraction. Single-crystal absorption spectra of **1** and of the mononuclear reference compound $K_3[Mn(CN)_6]$ in the near-IR region provide sound experimental evidence for the presence of low-spin Mn(III) ions ($S = 1$) with $^3T_1(t_{2g}^4)$ ground states in both compounds (Figure 1).[23]

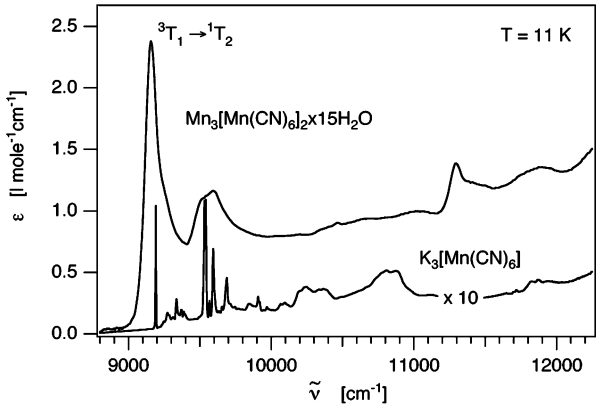

Figure 1. Single-crystal absorption spectra of **1** (top) and of $K_3[Mn(CN)_6]$ (bottom) in the near-IR spectral range. The latter spectrum is blown up by a factor of 10.

In $K_3[Mn(CN)_6]$, a series of sharp lines with an electronic origin at 9190 cm^{-1}, a well resolved vibronic structure, and a total oscillator strength of approximately 5×10^{-8} can be assigned to the spin-forbidden spin-flip transition $^3T_1(t_{2g}^4) \rightarrow {}^1T_2(t_{2g}^4)$.[24a,b] Compound **1** exhibits an absorption band at the same energy with a somewhat less resolved vibronic structure and an oscillator strength of 5×10^{-6}, approximately 100 times larger than that of the reference compound. The agreement between the two spectra clearly indicates the presence of C-bonded low-spin $[Mn(CN)_6]^{3-}$ chromophores in the PB-like phase of **1**. The considerably higher oscillator strength of the spin-flip band of the mixed valence compound as compared to the mononuclear compound is due to exchange interactions, which characteristically enhance the intensity of spin-forbidden transitions.[25] Therefore, the spectroscopic data together with electro-neutrality considerations lead to the formula $Mn(II)[Mn(III)(CN)_6]_{2/3}\cdot(6H_2O)_{1/3}\cdot yH_2O$, where y stands for the amount of zeolitic water.

The same conclusion follows from X-ray single-crystal analysis where the stoichiometric ratio x is determined directly (see Experimental section). The optimized value of x is 0.689(5), within 4 standard uncertainties of 2/3; the corresponding crystallographic agreement factor is $R_1 = 2.24\%$. A model with x fixed at 2/3 gives $R_1 = 2.28\%$, i.e., the increase in R-factor is insignificant; the model with x fixed at 3/4, corresponding to $Mn(III)[Mn(II)(CN)_6]_{3/4}\cdot(6H_2O)_{1/4}\cdot yH_2O$, gives $R_1 = 3.24\%$ and may thus be safely rejected. The same structural model refined from neutron powder data collected at 153 and 50 K gives $x = 0.60(2)$ and 0.62(2), respectively. Considering that population factors determined from powder patterns are

(17) Weber, T.; Estermann, M. A.; Bürgi, H. B. *Acta Crystallogr.* **2001**, *B51*, 559.
(18) Pejaković, D. A.; Manson, J. L.; Miller, J. S.; Epstein, A. J. *Phys. Rev. Let.* **2000**, *85*, 1994.
(19) Ziegler, B.; Witzel, M.; Schwarten, M.; Babel, D. *Z. Naturforsch.* **1999**, *54b*, 870.
(20) Herren, F.; Fischer, P.; Ludi, A.; Haelg, W. *Inorg. Chem.* **1980**, *19*, 956.
(21) Klenze, R.; Kanellakopulos, B.; Trageser, G.; Eysel, H. H. *J. Chem. Phys.* **1980**, *72*, 5819.
(22) Bushmann, W. E.; Miller, J. S. *Inorg. Chem.* **2000**, *39*, 2411.
(23) Figgis, B. N.; Hitchman, M. A. *Ligand Field Theory and Its Applications*; Wiley-VCH: New York **2000**.
(24) (a) Alexander, J. J.; Gray, H. B. *J. Am. Chem. Soc.* **1968**, *90*, 4260. (b) Jones, G. D.; Runciman, W. A. *Proc. Phys. Soc. (London)* **1960**, *76*, 996.
(25) McCarthy, P. J.; Güdel, H. U. *Coord. Chem. Rev.* **1988**, *88*, 69.

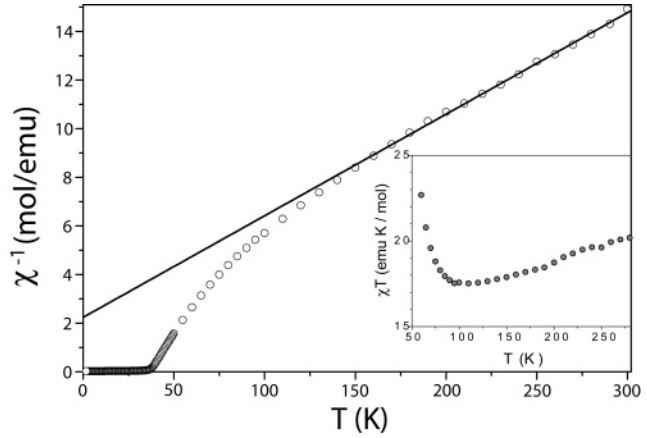

Figure 2. Temperature dependence of χ^{-1} and χT (insert) for **1** ($H = 10^3$ G). The inverse susceptibility shows Curie−Weiss behavior between 150 and 300 K (solid line).

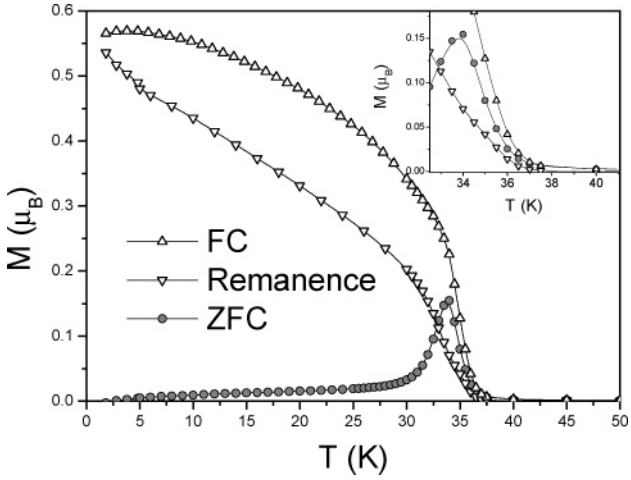

Figure 3. Temperature dependence of the ZFC, FC ($H = 5$ G) and remnant magnetizations of **1** (per unit cell). The insert shows these dependences near the magnetic phase transition.

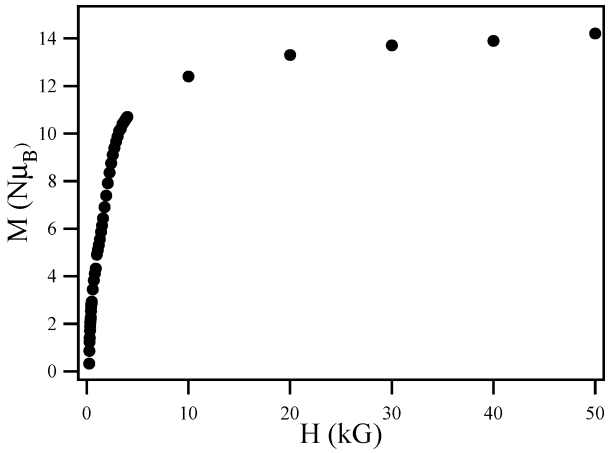

Figure 4. Field dependence of the magnetization M for **1** at $T = 1.8$ K (per unit cell).

generally less accurate than those from single-crystal data, the results from different diffraction experiments agree quite well.

The stoichiometry $Mn(II)[Mn(III)(CN)_6]_{2/3}\cdot(6H_2O)_{1/3}$ implies that on average Mn(II) is coordinated by four nitrogen atoms and two water molecules. The Mn(II)−N bond length from single-crystal structure analysis is 2.17 Å, the Mn(II)−O distance is 2.27 Å, while the Mn(III)−C distance is 1.97 Å. The bond lengths from the powder data are less accurate. These deviate somewhat from the single-crystal values, but they also show a difference between Mn(II)−N and Mn(III)−C distances in the range 0.15−0.3 Å. These distances imply that the ground state of the Mn(II) ions in the mixed N_4O_2 environment is high-spin $^6A_1(t_{2g}^3e_g^2, S = 5/2)$ while the Mn(III) ions are in a low-spin state $^3T_1(t_{2g},^4 S = 1)$, in agreement with the finding from optical spectroscopy.

The refined population y of zeolitic oxygen from single crystal ($T = 293$ K) and neutron powder experiments at 153 and 50 K is 3.1(1), 2.74(5), and 2.99(5), respectively. In general, for various batches of compound **1**, the total water content varies slightly, and the range was determined from a combination of elemental analyses, thermogravimetry and density measurements to correspond to $z = 12-16$ water molecules per formula unit $Mn(II)_3[Mn(III)(CN)_6]_2\cdot zH_2O$. For the specific case of the sample measured by X-ray single-crystal diffraction, the total water content $z = 3(6(1 - x) + 3y) = 15.3$ and for the sample measured by neutron powder diffraction $z = 15.4-15.8$.

Magnetism. We have studied the magnetic properties of **1** as a function of temperature and magnetic field by SQUID magnetometry and also probed its magnetic structure at 1.5 K by neutron powder diffraction. The main results are: (i) The dependence of χ^{-1} on T shows Curie−Weiss behavior in the temperature range 300−150 K with a negative Weiss constant $\Theta = -54$ K. The curve deviates from a straight line below 150 K and approaches a value of zero around 37 K. The temperature dependence of χT has a shallow minimum at around 100 K (Figure 2);

(ii) Upon heating, the magnetization of a sample cooled in zero-field (ZFC) has a value near zero at low temperatures, sharply increases at ∼32 K, reaches a maximum at 34 K and then decays to a value of zero at ∼37 K. The field cooled (FC) magnetization curve increases rapidly below 37 K to a maximum value of 0.57 μ_B per formula unit in a field of 5 G. When the field is switched off at 2 K, a remnant magnetization (RM) is observed, which vanishes above 37 K. Magnetic irreversibility (implying a visible difference between FC and ZFC magnetizations) also starts near 37 K (Figure 3);

(iii) At 1.8 K, the magnetization tends slowly toward a saturation value of 14 μ_B per unit cell as the field increases to 50 kG (Figure 4);

(iv) The occurrence of magnetic contributions to the neutron powder pattern at 1.5 K, with peaks at Bragg positions; the magnetic diffraction peaks have the same shape and width as the nuclear ones (Figure 5, (111) at $2\Theta \approx 17.5°$ and (311) at $2\Theta \approx 34°$).

Taken together, the experimental results (i−iv) are characteristic for ferrimagnetic behavior below the critical temperature $T_c \approx 35.5(2)$ K (see below). The narrow magnetic signals in the neutron powder pattern at 1.5 K (Figure 6) can be interpreted in terms of an ordered, collinear anti-ferromagnetic arrangement of adjacent magnetic moments of 4.87(13) and 2.20(17) μ_B for Mn(II) and Mn(III), respectively. These moments are close to the spin-only value for high-spin Mn(II), whereas for low-spin Mn(III), an orbital contribution has to be taken into account: $m_2 = \mu_B g_2 S_2^0 = 5\mu_B$ and $m_3 = \mu_B g_3 S_3^0 = 2.3\mu_B$.[28a] The saturated

(26) Ohkoshi, S.; Hashimoto, K. *Phys. Rev. B* **1999**, *60*, 12820.

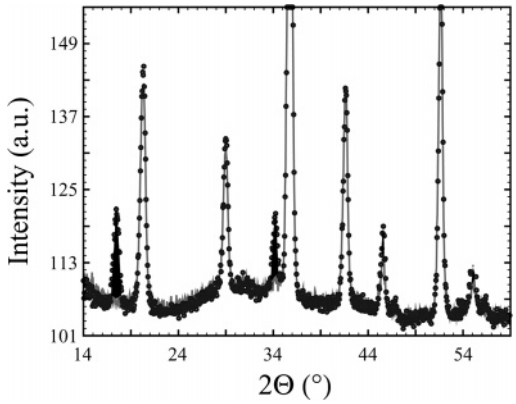

Figure 5. Part of the neutron powder patterns measured at 50 K (bold gray line) and 1.5 K (filled circles) for **1**. The black areas show the magnetic contributions.

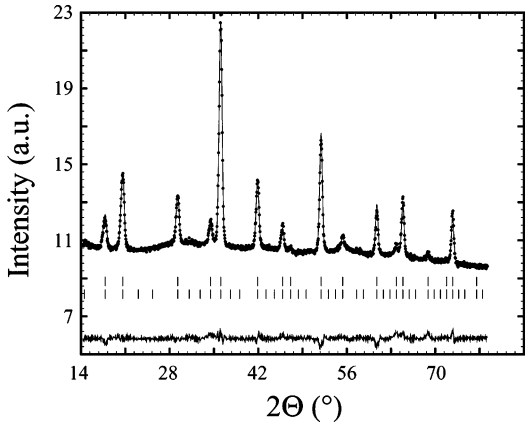

Figure 6. Observed (filled circles), calculated (line), and difference (bottom line) neutron powder diffraction patterns for **1** at $T = 1.5$ K (ferrimagnetic phase). The vertical bars show positions of Bragg reflections for nuclear (top) and magnetic (bottom) contributions allowed if the structural space group is $Fm\bar{3}m$ and the magnetic one $P\bar{1}$.

magnetization per unit cell containing four formula units of $Mn(II)[Mn(III)(CN)_6]_{2/3}\cdot(6H_2O)_{1/3}$ is

$$M_s = 4\left(m_2 \pm \frac{2}{3}m_3\right) = 4\mu_B\left(g_2S_2^0 \pm \frac{2}{3}g_3S_3^0\right) \qquad (2)$$

for ferro- (+) or antiferromagnetic (−) alignment of adjacent spins. For antiferromagnetic (−) alignment, it is calculated to be $13.9\mu_B$. This is close to the value of $14\mu_B$ observed by measuring the field dependence of the magnetization (Figure 4). To sum up, the negative Weiss constant, the nonlinear dependence of χ^{-1} on T in the low-temperature regime, and the shallow minimum in the χT curve (Figure 2) are also compatible with antiferromagnetic ordering.[26]

Unlike ZF magnetic Bragg scattering, the ZFC magnetization is nearly zero at low temperatures. This observation cannot be explained as a compensation of magnetizations from Mn(II) and Mn(III) magnetic sub-lattices. According to Molecular Field (MF) theory, the mean spin value per manganese site is[27]

$$\langle S_2\rangle = \frac{5}{2}B_{5/2}\left(\frac{5Z_2J_{23}}{k_BT}\langle S_3\rangle\right)$$

$$\langle S_3\rangle = B_1\left(\frac{2Z_3J_{23}}{k_BT}\langle S_2\rangle\right) \qquad (3)$$

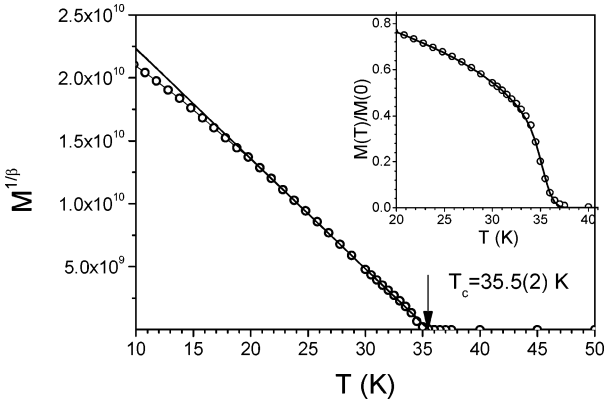

Figure 7. Critical behavior of the FC magnetization for **1**. The insert shows the comparison of experimental data (circles) and calculated FC magnetization (solid line) as a function of temperature (eq 4).

where B_S is the Brillouin function, $Z_2 = 4$ is the average number of magnetic neighbors of Mn(II), $Z_3 = 6$ is the number of magnetic neighbors of Mn(III). With an estimated exchange constant $J_{23} = 1.96$ cm^{-1},[28b] the sub-lattice and total magnetizations per unit cell between 35.5 and 0 K are calculated to increase monotonically from 0 to 20, −6 and 14 μ_B for Mn(II), Mn(III) and total magnetization, respectively. Thus, contrary to what has been found for other PB analogues, the stoichiometry of **1** excludes compensation of Mn(II) and Mn(III) magnetizations.[29]

To explain the ZFC behavior one could postulate a distribution of magnetically ordered domains whose moments compensate each other to give a vanishing bulk magnetization. At very low temperatures, the domains are sufficiently large to produce narrow magnetic Bragg reflections in magnetic neutron diffraction. Upon heating in a small field, competition between a thermally activated alignment of domains and a decrease of domain magnetization would account for the observed temperature dependence of the magnetization of the bulk sample.

The critical temperature and critical index of the magnetic phase transition has been determined from the scaling relation $M \propto (T_c - T)^\beta$ using the data between 20 and 30 K (solid line in Figure 7). The index β is 0.328(2), indistinguishable from the value $\beta = 0.326$ expected for a 3D Ising magnet.[30] The temperature dependence of magnetization shows a characteristic tail near T_c, obscuring its exact value. Convolution of the scaling law with a Gaussian distribution of local T_c's[31]

$$\frac{M(T)}{M(0)} = \int_T^\infty \frac{1}{\sqrt{2\pi}\Delta T_c}\exp\left(-\frac{(T_c - \langle T_c\rangle)^2}{2\Delta T_c^{\,2}}\right)\cdot\left(\frac{T_c - T}{T_c}\right)^\beta dT_c \qquad (4)$$

fits the experimental FC magnetization well for an average critical temperature $\langle T_c\rangle = 35.5$ K and a spread in critical

(27) Ohkoshi, S.; Iyoda, T.; Fujishima, A.; Hashimoto, K. *Phys. Rev. B* **1997**, *56*, 11642.
(28) (a) The quantities m_i, g_i and S_i^0 are the saturated magnetic moment, g-factor and spin value for an Mn^{i+} ion; $g_2 = 2$, $g_3 = 2.3$, $S_2^0 = 5/2$ and $S_3^0 = 1$. (b) The value of J_{23} was estimated from $k_BT_c = 2/3\sqrt{Z_2Z_3}J_{23}\sqrt{S_2(S_2+1)S_3(S_3+1)}$ to be J_{23}=1.96 cm^{-1} (2.6 K) at T_c=35.5 K. See Ohkoshi, S.; Hashimoto, K. *Chem. Phys. Let.* **1999**, *314*, 210.
(29) Ohkoshi, S.; Abe, Y.; Fujishima, A.; Hashimoto, K. *Phys. Rev. Lett.* **1999**, *82*, 1285.
(30) Campostrini, M.; Pelissetto, A.; Rossi, P.; Vicari, E. *Phys. Rev. E* **1999**, *60*, 3526.
(31) Grigoriev, S. V.; Klimko, S. A.; Kraan, W. H.; Maleyev, S. V.; Okorokov, A. I.; Rekveldt, M. T.; Runov, V. V. *Phys. Rev. B* **2001**, *64*, 94426.

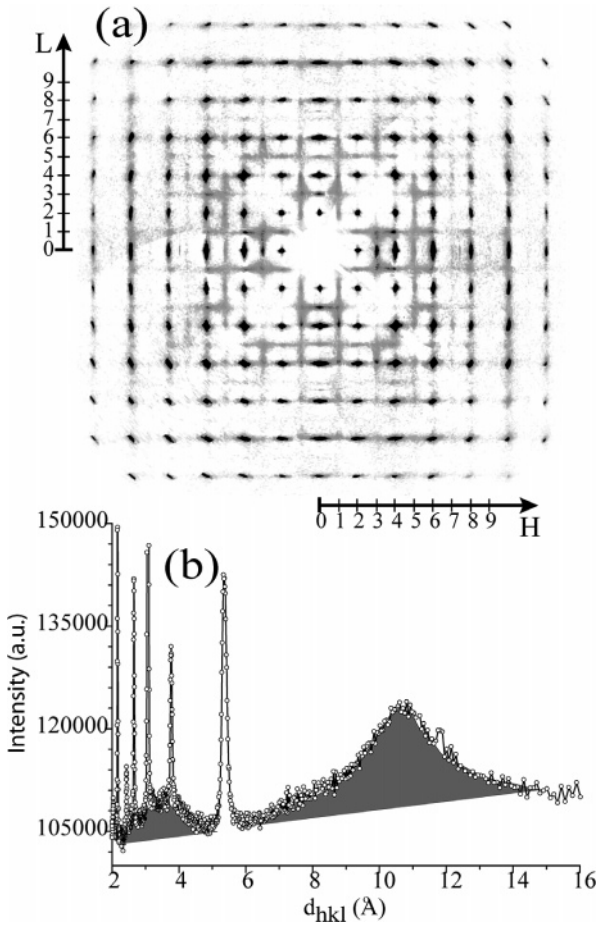

Figure 8. (a) Diffuse scattering of **1** obtained from a) single-crystal X-ray diffraction (H0L-layer, $T = 293$ K), (b) neutron powder diffraction (153 K). The gray areas in the powder diagram indicate diffuse contributions and correspond to the blurred features seen in a).

temperatures $\Delta T_c = 0.8$ K (Figure 7, insert). According to the theoretical concepts developed in refs 32−34 the spread in T_c may be interpreted in terms of long-range magnetic inhomogeneities.[31]

In summary, the magnetization measurements and magnetic neutron diffraction uncover antiferromagnetic ordering of the spins of adjacent manganese ions, appearing below 35.5 K, and leading to ferrimagnetic macroscopic behavior. The lack of bulk magnetization (at zero field) at low temperature together with magnetic Bragg scattering is indicative of magnetically ordered domains whose arrangement at zero field results in zero magnetization. More detailed information on the temperature evolution of the domain structure would require coercivity measurements in combination with neutron diffraction as a function of temperature. Such experiments are beyond the scope of this work.

Structural Disorder. Both single-crystal X-ray and neutron powder diffraction experiments reveal modulated diffuse scattering in addition to Bragg diffraction (Figure 8). The main diffuse features are independent of temperature as expected for irregular substitution of $[Mn(III)(CN)_6]^{3-}$ by $(H_2O)_6$. The neutron powder pattern exhibits a broad, but distinct diffuse peak centered on the position of the (100) reflection, which is forbidden in space group $Fm\bar{3}m$. The X-ray single-crystal diffraction data show structured diffuse scattering including rods and planes.

Layers equivalent under cubic symmetry (e.g., (*hk*0), (*h*0*l*), and (0*kl*), or (*hk*1), (*h*1*l*), and (1*kl*)) are practically undistinguishable, indicating that the symmetry of the diffuse scattering is cubic as well. Some diffuse features overlap, others do not overlap the Bragg reflections. The features at low resolution, the ones which determine the overall arrangement of the $M(CN)_6$ and $(H_2O)_6$ entities, occur in positions forbidden in an ordered $Fm\bar{3}m$ structure (Figure 8). They are not uniformly smeared out in reciprocal space, but are more or less concentrated along reciprocal lines. This distribution of diffuse intensity indicates short range order in the substitution pattern with primitive local translations, e.g., a propensity to form small pieces of chess board-like patterns composed of $[Mn(III)(CN)_6]^{3-}$ and $(H_2O)_6$ building blocks and oriented perpendicular to the *a*, *b*, or *c* axes. More accurate diffuse diffraction data are presently being collected from single crystals to allow a more quantitative analysis of disorder.

Experimental Section

The starting materials are commercially available and were used as purchased. The infrared spectrum of compound **1** dispersed in KBr was recorded on a FT-IR Spectrum One Spectrometer. The Raman spectrum was recorded on a small single crystal using a Spex Ramalog system and a Helium−Neon laser at 633 nm as excitation source. Low-temperature near-IR absorption spectra of single crystals of **1** (dimension $02 \times 0.2 \times 0.2$ mm^3) and $K_3[Mn(CN)_6]$ (dimension $6 \times 4 \times 3$ mm^3) between 8000 and 12 000 cm^{-1} were recorded on a FT instrument (Bruker IFS66) equipped with an appropriate beamsplitter, light-source and detector at a spectral resolution of 2 cm^{-1}. Temperatures down to 11 K were achieved with a closed cycle cryostat (Oxford Instruments CCC1100T). Magnetic susceptibility data were collected on a Quantum Design SQUID magnetometer (XL5S) equipped with a 50 kG magnet and operating in the temperature range 300−1.8 K. Pascal's constants were used for the diamagnetic corrections.

The X-ray single-crystal diffraction data were collected at $T = 293$ K with a Bruker CCD diffractometer. A standard hemisphere of reciprocal space was measured to a resolution of 0.758 Å by means of 0.3° ω-scans with Mo Kα radiation ($\lambda = 0.710\ 73$ Å) using SMART and integrated with SAINT.[35] Empirical absorption correction was made with SADABS,[36] structure refinement with SHELXL97[37] starting from a previously published model.[19] The final unconstrained refinement confirms the initial model with confidence factors $R_1 = 2.28\%$, w$R2 = 5.9\%$ and goodness of fit $\chi^2 = 1.227$.

The synchrotron single-crystal diffraction data ($T = 293$ K) were collected at the Swiss Norwegian Beam Lines located within the European Synchrotron Research Facility (SNBL ESRF) with a MAR image plate detector at room temperature with a wavelength of 0.7 Å. A full sphere was measured by

(32) Ginzburg, S. L. *JETP* **1977**, *46*, 1029.
(33) Korzhenevskii, A. L.; Heuer, H. O.; Herrmanns, K. *J. Phys. A.* **1998**, *31*, 927.
(34) Korzhenevskii, A. L.; Heuer, H. O.; Herrmanns, K. *Europhys.* Lett. **1999**, *45*, 195.
(35) SMART, Version 5.059 & SAINT, Version 6.02a Bruker AXS Inc., Madison, Wisconsin, USA, **2001**.
(36) Sheldrick, G. M.; SADABS, Version 2.06, Empirical Absorption Correction Program, University of Göttingen, Göttingen (Germany) **2002**.
(37) Sheldrick, G. M.; SHELXL97, University of Göttingen, Göttingen (Germany) **1997**.

means of 2° ω-scans to a resolution of 0.663 Å. Data were processed and reciprocal layers reconstructed from the raw data using CrysAlis software.[38]

The neutron diffraction experiments on polycrystalline **1** were performed on the HRPT diffractometer at SINQ, PSI in Villigen, Switzerland. The measurements were carried out at 1.5, 50, and 153 K with a closed-cycle He refrigerator and a wavelength $\lambda = 1.886$ Å (Ge monochromator). The 50 K diffraction pattern was refined starting from the X-ray single-crystal model and using the program FullProf.[39] Inclusion of the hydrogen atoms of the zeolitic water molecules in the structural model improved the refinement significantly. The agreement factors for 50 K (153 K) are $R_{\text{Bragg}} = 8.27\%$ (8.20%) and $\chi^2_{\text{Bragg}} = 17.0$ (8.87). The magnetic structure was established from the difference between the neutron diffraction patterns measured at 1.5 and 50 K after scaling the latter to the unit cell parameter corresponding to 1.5 K ($a = 10.5476(2)$ Å). This difference pattern was compared with calculated patterns using program FullProf.[39] Best agreement was obtained for a collinear antiferromagnetic arrangement of the high-spin Mn(II) and the low-spin Mn(III) moments. Finally, the magnetic moments of the manganese ions were refined from the 1.5 K diffraction pattern keeping the structural parameters fixed at the values corresponding to the 50 K data (Figure 7). The refinement was done in space group $Fm\bar{3}m$ for the nuclear and in space group $P\bar{1}$ for the magnetic structure. The agreement factors are $R_{\text{magnetic}} = 21.7\%$, $R_{\text{Bragg}} = 7.78\%$, and $\chi^2_{\text{Bragg}} = 10.9$.

Preparation of $K_3[Mn(CN)_6]$. The compound was prepared according to the literature procedure.[40]

Preparation of $Mn_3[Mn(CN)_6]_2 \cdot zH_2O$ (1). Slow diffusion of a solution of 12.60 g $MnCl_2 \cdot 4H_2O$ in 400 mL water in an Agar gel of 10.05 g Agar and 2.06 g KCN in 200 mL water under aerobic conditions, afforded within a few days, 0.86 g orange-red colored, transparent crystals showing a cubic morphology (38% yield based on KCN). IR (KBr): ν(CN) = 2148 cm^{-1}. Raman: ν(CN) = 2160 cm^{-1}. Anal. Calcd for $C_{12}H_{27}Mn_5N_{12}O_{13.5}$ (830.1): C 17.36, H 3.28, Mn 33.09, N 20.25. Found: C 17.72, H 3.17, Mn 33.2, N 19.69.

Conclusions

Optical spectroscopy, magnetometry, and high-resolution powder and single-crystal diffraction experiments have revealed the composition, oxidation states, crystal and magnetic structures of $Mn(II)[Mn(III)(CN)_6]_{2/3} \cdot (6H_2O)_{1/3} \cdot yH_2O$ (**1**). The compound maintains its inherently disordered crystal structure, which is face centered cubic on average only, down to 1.5 K, and without undergoing structural phase transformations. Intense diffuse scattering, which does not depend on temperature down to 1.5 K, has been observed in all diffraction experiments. The substitution of 1/3 of the $[Mn(III)(CN)_6]^{3-}$ ions by $(H_2O)_6$ clusters is not random, but shows short range order, possibly resulting from an alternation of $[Mn(III)(CN)_6]^{3-}$ and $(H_2O)_6$ building blocks. Near ~35.5 K, magnetic moments of adjacent Mn(II) and Mn(III) ions order antiferromagnetically. The FC magnetization shows scaling behavior typical for a 3D Ising magnet, but the transition is smeared with a spread of critical temperatures of about 0.8 K. At 1.5 K, the moments of adjacent manganese ions are nearly completely aligned and form macroscopic domains with long-range magnetic order. The ZFC magnetization is almost zero at 1.5 K; in the vicinity of 34 K it shows a peak and disappears above 37 K. We have suggested above that this temperature dependence may be related to formation of macroscopic domains below T_c. An alternative scenario proposed earlier for some Prussian Blue analogues on the basis of detailed SQUID measurements, namely spin cluster glass formation,[18,22] cannot be discarded on the basis of our data. The two scenarios may be differentiated experimentally: for a macroscopic domain structure, the magnetic Bragg reflections remain narrow up to temperatures near T_c, whereas the magnitude of the coercive field decreases exponentially with increasing temperature.[41] For a spin cluster glass, a broadening of magnetic diffraction features and a frequency dependence of the linear *ac* susceptibility should be observed. The occurrence of a temperature induced magnetic phase transition in the presence of a temperature independent structural disorder adds a further degree of complexity to this material. Again, analysis of diffuse scattering might provide experimental information on the interplay between these two features.

In conclusion, this study illustrates that despite its very simple average crystal structure, $Mn(II)[Mn(III)(CN)_6]_{2/3} \cdot (6H_2O)_{1/3} \cdot yH_2O$ shows a complex behavior at the microscopic, mesoscopic and macroscopic length scales. Experiments probing only average properties (microscopic and macroscopic) are insufficient to characterize such a compound in detail and will have to be complemented by methods probing the mesoscopic regime, e.g., by magnetic and nuclear diffuse scattering.

This work was supported by the Swiss NFP grant 4047-057532. The authors especially thank Dr. Hans Hagemann (University of Geneva) for the Raman measurement. Part of this work was performed at the Swiss Spallation Neutron Source, Paul Scherrer Institute, Villigen, Switzerland. Dedicated to Professor Philipp Gütlich on the occasion of his 70th birthday.

Supporting Information Available: One file containing crystallographic data in CIF format. This material is available free of charge via the Internet at http://pubs.acs.org.

JA0465451

(38) CrysAlis Software System, Version 1.171, Oxford-diffraction Ltd., Oxford (England) **2004**.
(39) Rodriguez-Carvajal, J. *Physica* **1993**, *B192*, 55.
(40) Buschmann, W. E.; Liable-Sands, L.; Rheingold, A. L.; Miller, J. S. *Inorg. Chimica Acta* **1999**, *284*, 175.
(41) Yusuf, S. M.; Raj, P.; Malik, S. K.; Sathyamoorthy, A.; Das, A.; Madhav Rao, L. *Solid State Comm.* **1999**, *112*, 207.